

Statistical approach for supernova matter.

A.S. Botvina^{a,b} and I.N. Mishustin^{b,c}

^a*Institute for Nuclear Research, Russian Academy of Sciences, 117312 Moscow, Russia*

^b*Frankfurt Institute for Advanced Studies, J.W. Goethe University, D-60438 Frankfurt am Main, Germany*

^c*Kurchatov Institute, Russian Research Center, 123182 Moscow, Russia*

Abstract

We formulate a statistical model for description of nuclear composition and equation of state of stellar matter at subnuclear densities and temperature up to 20 MeV, which are expected during the collapse and explosion of massive stars. The model includes nuclear, electromagnetic and weak interactions between all kinds of particles, under condition of statistical equilibrium. We emphasize importance of realistic description of the nuclear composition for understanding stellar dynamics and nucleosynthesis. It is demonstrated that the experience accumulated in studies of nuclear multifragmentation reactions can be used for better modelling properties of stellar medium.

PACS: 26.50.+x , 21.65.-f, 25.70.Pq , 26.30.-k, 97.60.Bw

1. Introduction

In violent nuclear reactions strong interaction between many nucleons leads to a fast equilibration. This short-range interaction is responsible for a sharp freeze-out when the inter-particle distance becomes larger than the interaction range. For these reasons statistical models have proved to be very successful for interpretation of nuclear reactions at various energies. They are widely used for description of fragment production when one or several equilibrated sources can be identified. Originally this concept was proposed for compound nucleus decays, such as evaporation or fission of excited nuclei [1]. Recently, it was demonstrated that the concept of equilibrated source can even be effectively used for more violent multifragmentation reactions leading to production of many fragments [2]. On other side, the statistical equilibrium is expected in many astrophysical processes, when the characteristic time for formation of nuclei is much shorter than the time-scale of these processes. For example, one of the most spectacular astrophysical events is a type II supernova explosion, with a huge energy release of about several tens of MeV per nucleon [3, 4]. When the core of a massive star collapses, it reaches densities several times larger than the normal nuclear density $\rho_0 = 0.15 \text{ fm}^{-3}$. The repulsive nucleon-nucleon interaction gives rise to a bounce-off and creation of a shock wave propagating through the

in-falling stellar material. This shock wave is responsible for the ejection of a star envelope that is observed as a supernova explosion. During the collapse and subsequent explosion the temperatures $T \approx (0.5 \div 10)$ MeV and densities $\rho \approx (10^{-6} \div 2)\rho_0$ can be reached. It is widely believed that the nuclear statistical equilibrium should be reached under these conditions. As shown by many theoretical studies, a liquid-gas phase transition should take place in nuclear matter under such conditions.

As discussed by several authors (see e.g. [5, 6, 7, 8]), there are problems in producing successful explosions in hydrodynamical simulations of the core-collapse supernovae, even when neutrino heating and convection effects are included. The hope is that full 3- d simulations will help to solve this problem [9]. On the other hand, it is known that nuclear composition is extremely important for understanding the physics of supernova explosions. In particular, the weak reaction rates and energy spectra of emitted neutrinos are very sensitive to the presence of heavy nuclei (see e.g. [10, 11, 12, 13]). This is also true for the equation of state (EOS) used in hydrodynamical simulations since the shock strength is diminished by dissociation of heavy nuclei.

Nuclear reactions in a supernova environment are especially important because supernova explosions may be considered as breeders for creating chemical elements. According to present understanding, there are three main sources of chemical element production in the Universe. The lightest elements (up to He, and, partly, Li) are formed during the first moments of the Universe expansion, immediately after the Big Bang. Light elements up to ^{16}O can be produced in thermonuclear reactions in ordinary stars like our Sun, while heavier elements up to Fe and Ni can be formed in heavy stars at the end of the nuclear burning epoch. It is most likely that heavy elements up to U were synthesized in the course of supernova explosions. Pronounced peaks in the element abundances can be explained by neutron capture reactions in s- and r-processes [14, 15]. It is believed that suitable conditions for the r-process were provided by free neutrons abundantly produced in supernova environments together with appropriate seed nuclei.

The EOS of supernova matter is under investigation for more than 25 years. One of the first EOS, frequently used in supernova simulations, was obtained in refs. [16, 17] many years ago. It includes both light and heavy nuclei in statistical equilibrium. However, it does not include the whole ensemble of hot heavy nuclei, replacing them by a single “average” nucleus. The same assumption within a relativistic mean-field approach was used in the EOS of ref. [18]. As was already pointed out by many authors [19, 20, 21, 22] this assumption is not sufficient for accurate treatment of the supernova processes. We think that this kind of approximation can distort the true statistical ensemble in many cases. There are other statistical calculations which consider the ensemble with different nuclear species, but in the partition sum they include only nuclei in long-lived states known from terrestrial experiments (see refs. [19, 21, 22]). Also, for description of unknown neutron-rich hot nuclei only properties (e.g., the symmetry energies) of cold and slightly excited isolated nuclei have been used up to now. These assumptions are not justified for supernova environments characterized by relatively high temperatures (up to 10 MeV) and densities of electrons and baryons in the range $\rho \approx 10^{-4} \div 10^{-1}\rho_0$. We believe, in order to achieve a more realistic description of supernova matter, it is necessary to

use rich experience accumulated in recent years by the nuclear community in studying highly excited equilibrated systems in nuclear reactions. In particular, multifragmentation reactions provide valuable information about hot nuclei in dense surrounding of nucleons and other nuclei, which in many aspects is similar to supernova interior [23].

2. Nuclear reactions in supernova environments.

2.1 Studying equilibrated nuclear matter in laboratory.

Properties of strongly-interacting nuclear matter are studied experimentally and theoretically for a long time. At present there exist consensus about phase diagram of nuclear and neutron matter (see, e.g., refs. [24, 25, 16]). It is shown schematically in Fig. 1 for symmetric nuclear matter, for range of densities and temperatures expected in the Supernova II explosions. It is commonly accepted that this diagram contains a liquid-gas phase transition. From this phase diagram one can conclude that nuclear matter at densities $\rho \approx 0.3 - 0.8\rho_0$ and temperatures $T < T_c$ should be in the mixed phase. This phase is strongly inhomogeneous with intermittent dense and dilute regions. In the case of electrically-neutral matter this mixed phase may have different topologies such as spherical droplets, cylindrical nuclei, slab-like configurations and others. These configurations are generally referred to as nuclear 'pasta' phases [26], which were recently under intensive theoretical investigation [27, 28, 29]. However, in the coexistence region at lower densities, $\rho < 0.3\rho_0$, which are considered in this paper, the nuclear matter breaks up into compact nuclear droplets surrounded by nucleons. These relatively low densities dominate during the main stages of stellar collapse and explosion. Description of nuclear composition in this region requires theoretical extrapolation of nuclear properties to these extreme conditions. As became obvious after intensive experimental studies of nuclear multifragmentation reactions, they proceed through formation of thermalized nuclear systems characterized by subnuclear densities $\rho \sim 0.1\rho_0$ and temperatures of 3–8 MeV. Thermodynamic conditions associated with these reactions are indicated by the shaded area in Fig. 1. This gives us a chance to extract properties of hot nuclei in the environment of other nuclear species directly from the experimental multifragmentation data and then use this information for more realistic calculations of nuclear composition of stellar matter. We have also shown isentropic trajectories with the entropy per baryon (S/B) of 1, 2, and 4 units (see section 5.2) typical for supernova explosions. One can see, for example, that an adiabatic collapse (and expansion) of stellar matter with typical entropies of 1-2 units per baryon passes exactly through the multifragmentation domain.

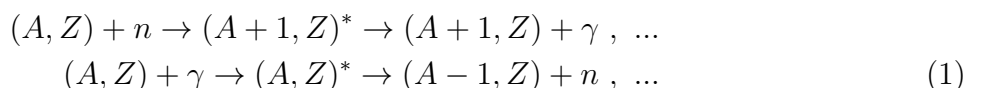
Nuclear multifragmentation, i.e. break-up of hot heavy nuclei into many fragments, was under intensive investigation during the last 20 years. It was solidly established by both theoretical and experimental studies that this channel dominates at high excitation energies, above 3–4 MeV per nucleon, replacing sequential evaporation and fission of the compound nucleus, which is conventional mechanism at low excitation energies. In this respect, multifragmentation is a universal process expected in all types of nuclear reactions, induced by hadrons, heavy ions, and electromagnetic collisions, where the nucleus

receives a high excitation energy. The Statistical Multifragmentation Model (SMM) [2] is one of the most successful models used for theoretical interpretation of these reactions. Some examples, how low-density equilibrated nuclear systems can be produced, and how well their decay can be described within this statistical approach, can be found in refs. [2, 30, 31, 32, 33, 34, 35, 36]. Recently, experimental evidences have appeared [37, 38, 39] that the symmetry energy of hot fragments produced in multifragmentation reactions is significantly reduced as compared with the value in cold nuclei. The surface and bulk energy of nuclei in this hot and dense environment can be modified too [40, 41]. These conclusions, made after appropriate analyses of experimental data, suggest that the same modifications will occur in stellar matter at similar densities and temperatures. Actually, the "in-medium" modifications are quite expected, since the nuclei will interact with the surrounding matter, and, therefore, should change their properties. These modifications may have important consequences for nuclear composition, equation of state, and weak reaction rates on these nuclei.

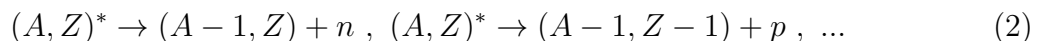
2.2 Nuclear and electro-weak reaction rates.

In the supernova environment, as compared to the nuclear reactions, several new important ingredients should be taken into consideration. First, the matter at stellar scales must be electrically neutral and therefore electrons should be included to balance a positive nuclear charge. Second, energetic photons present in hot matter may change nuclear composition via photo-nuclear reactions. And third, the matter is irradiated by a strong neutrino wind from the protoneutron star.

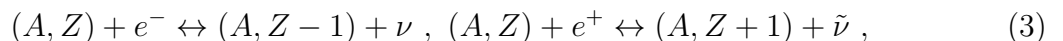
We consider macroscopic volumes of matter consisting of various nuclear species with mass number A and charge Z , (A, Z) , nucleons ($n = (1, 0)$ and $p = (1, 1)$), electrons (e^-) and positrons (e^+) under condition of electric neutrality. There exist several reaction types responsible for the chemical composition in supernova matter. At low densities and temperatures around a few MeV the most important ones are: 1) neutron capture and photodisintegration of nuclei, which proceed via production of a hot compound nucleus



2) neutron and light charged particle emission (evaporation) by the hot nuclei



and 3) weak processes induced by electrons/positrons and neutrinos/antineutrinos



which transfer protons to neutrons and vice versa. There are many other reactions not shown here, which are naturally taken into account within the assumption of statistical equilibrium. The characteristic reaction times for neutron capture, photodisintegration

of nuclei and nucleon emission are defined as

$$\begin{aligned}\tau_{\text{cap}} &= [\langle \sigma_{nA} v_{nA} \rangle \rho_n]^{-1} , \\ \tau_{\gamma A} &= [\langle \sigma_{\gamma A} v_{\gamma A} \rangle \rho_\gamma]^{-1} , \\ \tau_{n,p} &= \hbar / \Gamma_{n,p} ,\end{aligned}\tag{4}$$

respectively. Here σ_{nA} and $\sigma_{\gamma A}$ are the corresponding cross sections, v_{nA} and $v_{\gamma A}$ are the relative (invariant) velocities, and $\Gamma_{n,p}$ is the neutron (proton) decay width.

In our calculations for σ_{nA} we use the geometrical neutron–nuclear cross sections, that is a good approximation for the considered range of temperatures ($T \approx (0.5 \div 10)$ MeV). The photo–nucleus cross section $\sigma_{\gamma A}$ was taken phenomenologically under assumption that it is dominated by the giant dipole resonance. These parametrizations of neutron and photon cross-sections are in a good agreement with experimental data (see discussion in ref. [2]). The evaporation decay widths were calculated according to the Weisskopf evaporation model as described in ref. [42]. Our estimates show that at temperatures and densities of interest these reaction times vary within the range from 10 to 10^6 fm/c, that is indeed very short time scale compared to the characteristic hydrodynamic time of a supernova explosion, about 100 ms [5]. The nuclear statistical equilibrium is a reasonable approximation under these conditions.

We have calculated the reaction rates of Eq. (4) for nuclei with $A = 60$ and $Z = 24$, which are typical for stellar nucleosynthesis in dense matter and at a typical electron fraction (i.e., the ratio of electron and baryon densities ρ_e/ρ_B) $Y_e \sim 0.4$. They are presented in Fig. 2 as function of neutron density for several temperatures. By analyzing this figure one should take into account that the neutron density ρ_n is usually by 2–5 times smaller than ρ . One can see clearly that for densities $\rho_n > 10^{-5}\rho_0$ and for the expected temperatures of the environment, $T \lesssim 5$ MeV, we obtain $\tau_{\gamma A} \gg \tau_{\text{cap}}, \tau_{n,p}$, i.e. the photodisintegration is more slow than other processes. There exists a range of densities and temperatures, for example, $\rho_n \gtrsim 10^{-5}\rho_0$ at $T = 1$ MeV, $\rho_n \gtrsim 10^{-3}\rho_0$ at $T = 3$ MeV, and $\rho_n \gtrsim 10^{-2}\rho_0$ at $T = 5$ MeV, where the neutron capture dominates, i.e. $\tau_{\text{cap}} < \tau_{n,p}$. Under these conditions new channels for production and decay of nuclei will appear (e.g. a fast break-up with emission of α -particles or heavier clusters) which restore the detailed balance. We expect that in this situation an ensemble of various nuclear species will be in chemical equilibrium like in a liquid-gas coexistence region, as also observed in the multifragmentation reactions. Here the nuclear system is fully characterized by the temperature T , density ρ (which is nearly the same as baryon density ρ_B), and electron fraction Y_e . One may expect that modifications of nuclear properties come into force in this environment, because of intensive interaction between clusters. This is complementary to the well known effects in isolated nuclei: at high temperature the masses and level structure in hot nuclei can be different from those observed in cold nuclei (see, e.g., ref. [43]).

The weak interaction reactions are much slower. The direct and inverse reactions in Eq. (3) involve both free nucleons and all nuclei present in the matter. It is most likely that at early stages of a supernova explosion neutrinos/antineutrinos are trapped inside

the neutrinosphere around a protoneutron star [44]. In this case we should impose the lepton number conservation condition by fixing the lepton fraction Y_L . Then one should take into account the continuous neutrino flux out of the surface of the neutrinosphere propagating through the hot bubble. Due to large uncertainties in the weak interaction rates, below we consider three physically distinctive situations:

- 1) fixed lepton fraction Y_L corresponding to a β -equilibrium with trapped neutrinos inside the neutrinosphere (early stage of the explosion);
- 2) fixed electron fraction Y_e but no β -equilibrium inside a hot bubble (early and intermediate times);
- 3) full β -equilibrium without neutrino (the late times of the explosion, after neutrino escape).

The second case corresponds to a non-equilibrium situation which may take place in the bubble, before the electron capture becomes efficient. Actually, this case is considered as basic for calculations of nuclear composition in the hot bubble behind the shock. Generally, one should keep in mind that weak reactions are often out of equilibrium. Our estimates show that their characteristic times range from 10 ms to 10 s depending on thermodynamical conditions and intensity of the neutrino wind. Therefore, one should specify what kind of statistical equilibrium is expected with respect to weak interaction.

3. Formulation of the statistical model.

Below we describe supernova matter as a mixture of nuclear species, electrons, photons, and perhaps neutrinos in thermal equilibrium. For the macroscopic scales one can safely apply the grand-canonical approximation. We call this model the Statistical Model for Supernova Matter (SMSM). It was first proposed in ref.[20].

3.1 Equilibrium conditions.

Within the SMSM each particle i with baryon number B_i , charge Q_i and lepton number L_i is characterized by a chemical potential μ_i , which can be represented as

$$\mu_i = B_i\mu_B + Q_i\mu_Q + L_i\mu_L. \quad (5)$$

Here μ_B , μ_Q and μ_L are three independent chemical potentials which are determined from the conservation of total baryon number $B = \sum_i B_i$ electric charge $Q = \sum_i Q_i$ and lepton number $L = \sum_i L_i$ of the system. Explicitly, the chemical potentials for nuclear species (A, Z) , electrons (e^-, e^+) , and neutrinos $(\nu, \bar{\nu})$ can be expressed as

$$\begin{aligned} \mu_{AZ} &= A\mu_B + Z\mu_Q, \\ \mu_{e^-} &= -\mu_{e^+} = -\mu_Q + \mu_L, \\ \mu_\nu &= -\mu_{\bar{\nu}} = \mu_L. \end{aligned} \quad (6)$$

These relations are valid also for nucleons, $\mu_n = \mu_B$ and $\mu_p = \mu_B + \mu_Q$.

The corresponding conservation laws can be written as

$$\begin{aligned}\rho_B &= \frac{B}{V} = \sum_{AZ} A \rho_{AZ} , \\ \rho_Q &= \frac{Q}{V} = \sum_{AZ} Z \rho_{AZ} - \rho_e = 0 , \\ \rho_L &= \rho_e + \rho_\nu - \rho_{\bar{\nu}} = Y_L \rho_B .\end{aligned}\tag{7}$$

Here $\rho_e = \rho_{e^-} - \rho_{e^+}$ is the net electron density, Y_L is the lepton fraction. The second equation requires that any macroscopic volume of the star is electrically neutral.

The lepton number conservation is a valid concept only if ν and $\bar{\nu}$ are trapped in the system within the neutrinosphere [44]. If they escape freely from the system, the lepton number conservation is irrelevant and $\mu_L = 0$. In this case two remaining chemical potentials are determined from the conditions of baryon number conservation and electro-neutrality. Since the β -equilibrium may not be achieved in a fast explosive process, we also often fix the electron fraction $Y_e = \rho_e/\rho_B$ in this case.

3.2 Ensemble of nuclear species.

Our treatment of nuclear reactions is based on the statistical multifragmentation model (SMM) [2], which was very successfully applied for description of experimental data. For describing an ensemble of nuclear species under supernova conditions we use the Grand Canonical version of the SMM [45]. After integrating out translational degrees of freedom one can represent pressure of nuclear species as

$$P_{\text{nuc}} = T \sum_{AZ} \rho_{AZ} \equiv T \sum_{AZ} g_{AZ} \frac{V_f}{V} \frac{A^{3/2}}{\lambda_T^3} \exp \left[-\frac{1}{T} (F_{AZ} - \mu_{AZ}) \right] ,\tag{8}$$

where ρ_{AZ} is the density of nuclear species with mass A and charge Z . Here g_{AZ} is the ground-state degeneracy factor of species (A, Z) , $\lambda_T = (2\pi\hbar^2/m_N T)^{1/2}$ is the nucleon thermal wavelength, $m_N \approx 939$ MeV is the average nucleon mass. V is the actual volume of the system, and V_f is so called free volume, which accounts for the finite size of nuclear species. We assume that all nuclei have normal nuclear density ρ_0 , so that the proper volume of a nucleus with mass A is A/ρ_0 . At low densities the finite-size effect may be included via the excluded volume approximation $V_f/V \approx (1 - \rho_B/\rho_0)$. We emphasize that this last approximation is commonly accepted in statistical models. As we know from nuclear multifragmentation studies information about free volume can be extracted from analysis of experimental data [32]. At densities $\rho_B > 0.1\rho_0$ the extracted V_f may slightly deviate from above approximation, however, they are in qualitative agreement. In the present work we remain in the framework of the conventional statistical approach, although allowing for modifications of nuclear properties.

The internal excitations of nuclei play an important role in regulating their abundance, since they increase significantly their entropy. Some authors (see, e.g., ref. [19]) limit the

excitation spectrum by particle-stable levels known for low excited nuclei. Within the SMM we follow quite different philosophy. Namely, we calculate internal excitation of nuclei by assuming that they have the same internal temperature as the surrounding medium. In this case not only particle-stable states but also particle-unstable states will contribute to the excitation energy and entropy. This can be justified by the dynamical equilibrium of nuclei in hot environment, and supported by numerous comparisons with experiment (see part **2.1**). Moreover, in the supernova environment both the excited states and the binding energies of nuclei will be strongly affected by the surrounding matter. By this reason, we find it more appropriate to use an approach which can easily be generalized to include in-medium modifications. Namely, the internal free energy of species (A, Z) with $A > 4$ is parameterised in the spirit of the liquid drop model, which has been proved to be very successful in nuclear physics [1]:

$$F_{AZ}(T, \rho) = F_{AZ}^B + F_{AZ}^S + F_{AZ}^{\text{sym}} + F_{AZ}^C . \quad (9)$$

Here the right hand side contains, respectively, the bulk, the surface, the symmetry and the Coulomb terms. The first three terms are taken in the standard form [2],

$$F_{AZ}^B(T) = \left(-w_0 - \frac{T^2}{\varepsilon_0} \right) A , \quad (10)$$

$$F_{AZ}^S(T) = \beta_0 \left(\frac{T_c^2 - T^2}{T_c^2 + T^2} \right)^{5/4} A^{2/3} , \quad (11)$$

$$F_{AZ}^{\text{sym}} = \gamma \frac{(A - 2Z)^2}{A} , \quad (12)$$

where $w_0 = 16$ MeV, $\varepsilon_0 = 16$ MeV, $\beta_0 = 18$ MeV, $T_c = 18$ MeV and $\gamma = 25$ MeV are the model parameters which are extracted from nuclear phenomenology and provide a good description of multifragmentation data [2, 31, 32, 33, 34, 35, 36]. However, these parameters, especially the symmetry coefficient γ , can be different in hot nuclei at multifragmentation conditions, and they should be determined from corresponding experimental observables (see discussion in refs. [40, 41, 46]).

In the electrically-neutral environment the nuclear Coulomb term should be modified to include the screening effect of electrons. Within the Wigner-Seitz approximation with constant electron density it can be expressed as

$$F_{AZ}^C(\rho) = \frac{3}{5} c(\rho) \frac{(eZ)^2}{r_0 A^{1/3}} , \quad (13)$$

$$c(\rho) = \left[1 - \frac{3}{2} \left(\frac{\rho_e}{\rho_{0p}} \right)^{1/3} + \frac{1}{2} \left(\frac{\rho_e}{\rho_{0p}} \right) \right] ,$$

where $r_0 = 1.17$ fm and $\rho_{0p} = (Z/A)\rho_0$ is the proton density inside the nuclei. The screening function $c(\rho)$ is 1 at $\rho_e = 0$ and 0 at $\rho_e = \rho_{0p}$. Here one can also use an approximation $\rho_e/\rho_{0p} = \rho_B/\rho_0$, as in ref. [16]. In our calculations, we have checked that

these two choices lead to very similar results, especially at small densities. We want to stress that both the reduction of the surface energy due to the finite temperature and the reduction of the Coulomb energy due to the finite electron density favour the formation of heavy nuclei. Nucleons and light nuclei ($A \leq 4$) are considered as structure-less particles characterized only by exact masses and proper volumes [2]. Their Coulomb interaction is taken into account within the same Wigner-Seitz approximation.

As follows from Eq. (8), the fate of heavy nuclei depends strongly on the relationship between F_{AZ} and μ_{AZ} . In order to avoid an exponentially divergent contribution to the baryon density, at least in the thermodynamic limit ($A \rightarrow \infty$), inequality $F_{AZ} \gtrsim \mu_{AZ}$ must hold. The equality sign here corresponds to the situation when a big (infinite) nuclear fragment coexists with the gas of smaller clusters [47]. When $F_{AZ} > \mu_{AZ}$, only small clusters with nearly exponential mass spectrum are present. However, there exist a region of thermodynamic quantities corresponding to $F_{AZ} \approx \mu_{AZ}$ when the mass distribution of nuclear species is a power-law $A^{-\tau}$ with $\tau \approx 2$. The advantage of our approach is that we consider all the fragments present in this transition region, contrary to the previous calculations [16, 17], which consider only one ‘‘average’’ nucleus characterizing the liquid phase.

3.3 Electromagnetic and weak processes.

At $T, \mu > m_e$ the pressure of the relativistic electron-positron gas can be written as

$$P_e = \frac{g_e \mu_e^4}{24\pi^2} \left[1 + 2 \left(\frac{\pi T}{\mu_e} \right)^2 + \frac{7}{15} \left(\frac{\pi T}{\mu_e} \right)^4 - \frac{m_e^2}{\mu_e^2} \left(3 + \left(\frac{\pi T}{\mu_e} \right)^2 \right) \right], \quad (14)$$

where first-order correction ($\sim m_e^2$) due to the finite electron mass is included, $g_e=2$ is the spin degeneracy factor. The net number density ρ_e and entropy density s_e can be obtained from standard thermodynamic relations, $\rho_e = \partial P_e / \partial \mu_e$, and $s_e = \partial P_e / \partial T$, which give

$$\rho_e = \frac{g_e}{6\pi^2} \left[\mu_e^3 + \mu_e \left(\pi^2 T^2 - \frac{3}{2} m_e^2 \right) \right], \quad (15)$$

$$s_e = \frac{g_e T \mu_e^2}{6} \left[1 + \frac{7}{15} \left(\frac{\pi T}{\mu_e} \right)^2 - \frac{m_e^2}{2\mu_e^2} \right]. \quad (16)$$

Electron neutrinos and antineutrinos are taken into account in the same way, but as massless fermions, and with the degeneracy factor twice smaller than for the electrons, i.e., $g_\nu=1$. The photons are always close to the thermal equilibrium, and they are treated as massless Bose gas with zero chemical potential. The corresponding density ρ_γ , energy density e_γ , pressure P_γ , and entropy density s_γ of photons gas are given by standard formulae:

$$\rho_\gamma = \frac{g_\gamma \xi(3) T^3}{\pi^2 \hbar^3 c^3}, \quad e_\gamma = \frac{g_\gamma \pi^2 T^4}{30 \hbar^3 c^3}, \quad P_\gamma = \frac{e_\gamma}{3}, \quad s_\gamma = \frac{4e_\gamma}{3T}, \quad (17)$$

where $g_\gamma=2$.

All kinds of particles (nuclei, baryons, electrons, neutrinos, photons) contribute to the free energy, pressure and other thermodynamical characteristics of the system, and we sum up all these contributions. Within the model we calculate densities of all particles self-consistently by taking into account the relations between their chemical potentials.

3.4 Comparison with the Lattimer-Swesty model.

We have performed calculations for sets of physical conditions expected during the collapse of massive stars and subsequent supernova explosions. We take baryon number $B = 1000$ and perform calculations for all fragments with $1 \leq A \leq 1000$ and $0 \leq Z \leq A$ in a box of fixed volume V . This volume is determined by the average baryon density $\rho_B = B/V$. This restriction on the size of nuclear fragments is fully justified in our case, since fragments with larger masses ($A > 1000$) can be produced only at very high densities $\rho \gtrsim 0.5\rho_0$ [4, 16], which are appropriate for the regions deep inside the protoneutron star, and which are not considered here.

In the beginning we compare our model with calculations within other models on the market. It is necessary to mention that all models treat electrons and photons in the same way, therefore, differences appear entirely due to different description of nuclear species. One can expect that in the case of domination of radiation processes the results will be similar.

Most supernova simulations are performed with the equation of state of Lattimer-Swesty (LS) [16, 17], where an ensemble of heavy nuclei is replaced by a single “average” nucleus. Therefore, one can compare only integral characteristics of the stellar matter. In Fig. 3 we compare our SMSM results with the LS model. We show entropies, pressure, mass fractions of alpha particles (X_{alpha}), and heavy fragments (X_{heavy}), at different temperatures, and at a fixed electron fraction, versus densities. In the SMSM X_{heavy} includes all fragments with $A > 4$, whereas in the LS model it is only the share of the “average” heavy nucleus. The LS calculations were taken from ref. [22]. One can see that the average thermodynamical characteristics (pressure, entropy) are very close in the two models. This remains also true if we extend comparison to other models, e.g., reported in [22, 19]. However, as seen from Fig. 3, mass fractions of nuclei are very different. As was mentioned in [22], a small yield of alpha clusters in the LS model may be caused by mistakes in calculations of the Coulomb corrections to their binding energies. We stress again that the details of the nuclear composition are very important for dynamics of the explosion, since it influences the total energy balance, and determines the weak reaction rates.

4. Composition of matter.

In this section we present the SMSM results concerning nuclear and lepton composition of stellar matter, which are important for determining general thermodynamical characteristics of the matter, such as energy density, pressure, and entropy. The energy deposition into the matter with photons and neutrinos produced by external sources is

also considerably influenced by this composition. We pay special attention to the contribution of nuclear species whose properties may be modified in dense environment as follows from recent findings in nuclear multifragmentation reactions.

4.1 Electron and neutron fractions of stellar matter.

Within the SMSM we can calculate the electron fraction in the electrically-neutral matter under assumption of full β -equilibrium. The appropriate astrophysical sites, where this may happen, are the relatively slow collapse stage, and the very late stages of the explosion, after cooling down the matter and neutrino escape. In this case we calculate self-consistently densities of all species by using relations between their chemical potentials, Eq. (6), with $\mu_L=0$. The net electron density, which is equal to the proton density, is explicitly given as a function of the chemical potential in Eq. (15). Fig. 4 presents the fractions of free electrons and neutrons as functions of baryon density.

On the left panels the results are shown for the β -equilibrium neutrino-less matter at $T=1$ and 3 MeV. One can clearly see two general trends: with increasing baryon density the electron fraction Y_e gradually decreases and the neutron fraction Y_n increases. At small densities, which correspond to low μ_e , the electrically-neutral matter tends to be isospin symmetric, with a large amount of electrons. In the case of low temperatures ($T \lesssim 1$ MeV) the protons are captured in most bound nuclei with $A \sim 50$ –60. As was realized long time ago [4], at large densities the electrons are absorbed by protons in the inverse β -decay process, that is driven by high electron chemical potential. When we increase temperature ($T \gtrsim 3$ MeV) the nuclei dissociate into protons and neutrons, that helps to capture electrons at large densities also. At the same time, the number of free neutrons increases rapidly at higher baryon densities for both low and high temperatures. This is important for maintaining a high rate of nuclear reactions to generate equilibrium ensemble of nuclei. At low temperatures ($T \sim 1$ MeV) a noticeable change in the trend is seen below $\rho_B \approx 10^{-4}\rho_0$. At these densities most neutrons are bound in large nuclei, which are still present in the matter. For example, $Y_n \approx 0.2$ means that 80% of neutrons are trapped in the nuclei. At even lower densities, when heavy nuclei disappear (see Fig. 3) the number of free neutrons increases. The same trend at higher densities is explained by the fact that more and more neutrons are dripping out of nuclei, since the matter contains less and less protons. For example, at $\rho_B > 10^{-3}\rho_0$ more than half of the neutrons are free. This behavior correlates with decreasing the number of electrons and a relatively small share of heavy nuclei in the system. At higher densities, the structure of matter may change because of the neutrino/antineutrino and electron/positron capture reactions [4].

The right panel of Fig. 4 shows the results obtained under the condition of lepton number conservation, i.e., at fixed values of lepton fractions $Y_L=0.1, 0.2, 0.3$. These values are consistent with uncertainties concerning the neutrinosphere radius discussed in literature. One can see that in this case the number of free neutrons always drops with density reflecting formation of very big nuclei and transition to the liquid phase at $\rho_B \rightarrow \rho_0$. While the electron fraction stays nearly constant, exhausting around 80–90% of

the total Y_L . These results show that weak reactions affect significantly the composition of supernova matter.

4.2 Mass fractions of light and heavy nuclei.

As well known, at low densities and temperatures the nuclear matter exists in the form of isolated nuclei and nucleons. At terrestrial conditions the nuclei capture electrons and become atoms. However, at supernova conditions the atoms are fully ionized, therefore, the nuclei are embedded in more or less uniform background of electrons and neutrons. This surrounding to a large extent determines the nuclear composition of stellar matter.

Figures 5 and 6 demonstrate the mass fractions of nuclear matter contained in heavy nuclei (with mass numbers $A > 4$), α -particles, neutrons and protons, for different electron fractions Y_e . One can see that at low temperatures ($T < 1$ MeV) the matter is mainly composed of heavy nuclei. If the share of electrons is small, the free neutrons are also present. With increasing temperatures the heavy nuclei gradually disintegrate into α 's, neutrons and protons. At low densities this disintegration happens already at moderate temperatures $T \sim 1$ – 2 MeV, while at subnuclear densities ($\rho \sim 0.1\rho_0$) the heavy nuclei survive even at higher temperatures, though they become very excited. One should bear in mind, however, that in this case we are dealing with the dynamical equilibrium between decay of excited nuclei and absorption of surrounding nucleons, as regulated by the reaction rates presented in Fig. 2. An interesting observation is that heavy nuclei first break-up into light clusters (like α) and then these clusters dissolve into nucleons with temperature. This is clear seen in the yields of α -particles, which demonstrate a 'rise and fall' behaviour both with increasing temperature and decreasing density. As seen from Figs. 7 and 8, small clusters with $A=2$ and 3 are also produced in the transition region.

4.3 Nuclear mass distributions.

The properties of heavy nuclei are very important for understanding processes taking place in stellar matter. In the bottom panel of Fig. 7 we show mass distributions of nuclear species at $\rho_B = 10^{-3}\rho_0$ and several temperatures. At low temperatures the distribution of heavy nuclei looks like a Gaussian with a well defined peak (see also ref. [20]). In this case the average thermodynamic characteristics of the system may not be much different from the ones calculated under assumption of an "average" nucleus as in ref. [17], see Fig. 3. However, even in this case, the width of the distributions may be important for calculations of weak reactions in matter. By increasing temperature we move into a coexistence region of the nuclear liquid-gas phase transition: The mass distributions become 'U-shaped', and they contain all nuclei from light to heavy ones. At higher temperatures the mass distributions have exponential shape. These distributions can not be even approximately characterized by an "average" nucleus. This evolution of fragment mass distributions is well established in nuclear multifragmentation reactions [2, 36].

The average charge-to-mass ratio for all nuclei is demonstrated in the top panel of Fig. 7. For this quantity both the symmetry and Coulomb energies of fragments are

crucially important. The charges of heavy fragments show rather regular behaviour: The Z/A ratio decreases slowly with mass number because of Coulomb interaction. It decreases less rapidly than in multifragmentation reactions due to the screening effect of electrons. From our calculations we came to the conclusion that the charge distribution of nuclei at given A can be approximated by a Gaussian, with the width $\sigma_Z \approx \sqrt{AT/8\gamma}$ [42, 45, 48], where γ is the coefficient in the symmetry energy (see Eq. (12)).

We have found that the phase transition from heavy nuclei to light fragments (nuclear gas) always proceeds through the same sequence of mass distributions: 'U-shape', power-law, and exponential ones, both with increasing temperature and decreasing density. This opens the possibility to study the critical behaviour in stellar matter, in the same way as was previously done in multifragmentation reactions [32, 36]. One can find examples of the temperature-driven transitions in refs. [20, 23] and in Fig. 7 (see also Fig. 22). In Fig. 8 we demonstrate an example of the density-driven transition at fixed temperature of 1 MeV. As we can clearly see, the mass distributions evolve from 'U-shape' at densities (in units $10^{-5}\rho_0$) 1.0 and 0.32 to power-law at 0.18 and 0.1, and finally to exponential at 0.03. At density 0.18 the distribution of large clusters is most flat, that may be considered as a critical point of the phase transition [47].

4.4 Shell effects.

Up to now we have used the liquid-drop description of nuclei in the stellar matter. However, it is well known that at low temperatures ($T \lesssim 1$ MeV) the shell corrections to nuclear masses becomes important, at least, at terrestrial densities of matter. It is likely that the shell effects may also play a role in stellar matter at subnuclear densities. In this section we demonstrate how shell effects may influence the mass and charge distributions of nuclei. In particular, we have analyzed possible existence of superheavy elements in stellar matter, assuming that they are sufficiently long-lived. It was assumed that there is a certain shell correction to the free energy F_{AZ} of a specific nucleus, ΔF_{AZ} , taken as follows:

$$\Delta F_{AZ} = - \left[E_{sh} \exp \left(- \frac{(N - N_{sh})^2}{2\sigma_N^2} \right) + E_{sh} \exp \left(- \frac{(Z - Z_{sh})^2}{2\sigma_Z^2} \right) \right]. \quad (18)$$

We have assumed existence of the island of stability around $Z_{sh}=120$ and $N_{sh}=180$ [49]. The maximum energy of the shell correction is chosen to be $E_{sh}=5$ MeV, and the widths of the shell are $\sigma_N = \sigma_Z = 5$ MeV. These values are consistent with the magnitudes of the shell effects discussed for superheavy elements. In Fig. 9 we compare the calculated charge and mass distributions without and with the shell corrections (i.e., without and with the term ΔF_{AZ}). We consider typical conditions in supernova matter where the production of superheavy nuclei is still possible, i.e., $T=1$ MeV, $\rho_B \approx 0.05\rho_0$, $Y_e = 0.2$. One can see that a pure liquid-drop description predict Gaussian-like mass and charge distributions of fragments which move to smaller values with decreasing density. When the shell constraint is imposed, the yields become essentially, by factor 2–5, larger in the vicinity of neutron (N_{sh}) and proton (Z_{sh}) 'magic' numbers. Moreover, because of the

increased binding, these magic nuclei are abundantly produced in a rather broad region of density. For example, the neutron shell of $N_{sh}=180$ dominates clearly at densities of both $0.03\rho_0$ and $0.05\rho_0$.

This result makes possible to discuss nucleosynthesis of superheavy elements at supernova conditions. As has been already pointed out in ref. [20], there is a chance that heavy nuclei could be produced at subnuclear densities, and then ejected into the space. At considered small temperature (1 MeV) the effect of secondary deexcitation will be minimal, only few nucleons will be lost. The fission channels for these neutron-rich nuclei may also be suppressed by the shell effects [50] and electron screening [51]. However, one can expect that these nuclei will fastly emit neutrons above the neutron drip-line, undergo abundant β decay and, possibly, α emission. We are planning to analyze all these processes in the forthcoming publications [52]. Here we mention only a possible scenario how such superheavy nuclei can be ejected into space. Since the synthesis of heavy and superheavy nuclei is only possible at rather high baryon density $\rho_B \sim 0.05\rho_0$ it is most likely that such nuclei will not be ejected in the course of the supernova explosion. Instead, they will be accumulated at the surface of a newly produced neutron star. If this star is in a binary system with another neutron star, white dwarf, or even a black hole, there is a chance of their collision at later stages of evolution. Then a part of the stellar material will be ejected in space, while the other part may collapse into a black hole. One can also speculate about asymmetric explosions of supernovas, acceleration of nuclei by the neutrino wind, and starquakes which may provide this ejection (see, e.g., refs. [53, 54, 55]). The search for new mechanisms of nucleosynthesis is motivated by the fact that the traditional s - and r -processes have serious problems to explain synthesis of fissioning nuclei larger than lead [15].

5. Thermodynamical characteristics of stellar matter.

In this section we present general thermodynamical characteristics of stellar matter, such as energy density, pressure and entropy as functions of temperature T , baryon density ρ_B , electron fraction Y_e , as well as the nuclear composition. In hydrodynamical simulations most important role is played by Equation of State (EOS), which connects pressure with the energy density. The dynamics of collapse and explosion depends essentially on the EOS [5].

5.1 Caloric curve, pressure and entropy

One of the main inputs for dynamical simulations of supernova explosions is the total thermal energy deposited in the matter. In Fig. 10 we show so-called caloric curves, i.e., the thermal energy per nucleon of the matter as a function of temperature. For convenience, the actual energy per nucleon is shifted by the value of 16 MeV, which corresponds to the bulk binding energy of nuclear matter at $\rho_B = \rho_0$. Our calculations show that nuclear contributions dominate at high densities and low temperatures, where heavy nuclei survive. Due to the internal excitation of these nuclei according to the

compound nucleus law, $E^* \sim T^2$, the caloric curve has a parabolic shape at $\rho_B \sim 0.1 - 0.001\rho_0$. However, at low densities and high temperatures electrons and photons dominate, and the caloric curve behaves according to the Stefan–Boltzmann law $E^* \sim T^4$, i.e., the energy per nucleon grows very rapidly with temperature. One can also see that the nuclear contributions become nearly independent on baryon density at high temperatures. Namely, they approach the Boltzmann limit, $E^* \sim 1.5T$, when nuclear matter disintegrate completely into nucleons. It is instructive to note that at high densities $\rho \sim 0.1\rho_0$ and proton fractions $Y_p = Y_e \sim 0.4$ which are typical for normal nuclei, the caloric curve is determined mainly by the nuclear species, and it reminds very much the caloric curves extracted from the multifragmentation reactions [2]. In this case, the excitation energy increases rapidly at temperatures $T \approx 4 - 6$ MeV, which correspond to the maximum in the heat capacity. This is a characteristic feature of the liquid-gas phase transition [36, 47].

Pressure is another important characteristic of the matter, which, in competition with the gravitational pressure, determines the structure and dynamics of the stellar system. In Figs. 11 and 12 we plot the pressure versus baryon density for different temperatures. There are several important features to be mentioned. First, the nuclear contributions are mainly important in the intermediate density region $(10^{-4} - 10^{-2})\rho_0$, where, depending on temperature, more and more free nucleons are present in the nuclear matter. In the case of full disintegration of nuclear species into nucleons, the nucleons may contribute up to 50% to the total pressure. Second, at higher densities the pressure is dominated by the relativistic electrons, since their chemical potential becomes very high. Third, at very low densities and high temperatures the radiation pressure dominate, which is proportional to T^4 and does not depend on baryon density. One can see that the nuclear pressure is higher in the case of a low electron fraction ($Y_e=0.2$), because of a considerable abundance of free neutrons, even if large nuclei are present in the matter. In the modern hydrodynamical simulations of supernova explosions the shock stalls at densities around $10^{-6} - 10^{-5}\rho_0$ [5]. This happens partly because a significant fraction of shock energy is used for disintegration of infalling nuclei, from C to Fe. Therefore, survival of medium and heavy nuclei would contribute essentially to the revival of the shock.

The entropy per baryon S/B , which is shown in Fig. 13 as a function of temperature, is an important characteristic of the exploding matter. One can notice that it correlates strongly with behavior of the caloric curve. At low temperatures and high densities the nuclear contribution to the entropy dominates. At high temperatures, the nuclei disintegrate into nucleons and the nuclear entropy depends only logarithmically on temperature and density according to the Boltzmann gas law. Usually, at entropy greater than 10 units per nucleon only nucleon gas without heavy nuclei is present in the system. The main contribution to the total entropy in this case is provided by the radiation and electron-positron pairs. This contribution does not depend on density and is proportional to T^3 . The total entropy has a jump across the shock, which can be explained in part by disintegration of heavy nuclei. Therefore, even small differences in nuclear properties in medium, in comparison with isolated nuclei, may lead to significant effects in the shock dynamics.

5.2 Adiabatic trajectories.

Some important processes in stellar matter proceed with approximately constant entropy. For example, the collapse of a massive star before re-bounce is characterized by the entropy around one unit per nucleon. After propagation of the shock wave the entropy increases drastically. However, subsequent evolution of the matter is again close to isentropic, and this assumption is quite valid for nucleosynthesis. For this reason we consider adiabatic trajectories in the $T - \rho_B$ plane, and calculate fragment mass distributions and thermodynamical functions along these trajectories.

In Fig. 14 we show adiabatic trajectories for several fixed S/B . This representation of the phase diagram on $T - \rho$ plane is very convenient for understanding thermodynamical properties of stellar matter (compare also with Fig. 1). It is also possible to make a rough estimation of nuclear composition of the matter: As well known from previous studies [4], at $S/B=1$ many heavy nuclei exist in the matter, while at the entropy as high as $S/B=20$ the baryonic matter consist mainly of free nucleons and hadron resonances. Our calculations confirm this expectation.

It is instructive to compare mass fractions of different nuclear species along the adiabats for different thermodynamical conditions, in order to get an idea about evolution of nuclei during the whole collapse–explosion process. In Fig. 15 we show these fractions (similar to Fig. 6) for $S/B=1$, where the mass fraction of heavy nuclei is close to 1, and for $S/B=8$, where the nuclei undergoes deep disintegration. In the latter case the fraction of nuclei with $A > 4$ is essential only at high densities, and there are no large fragments at low densities. At $S/B=8$ the fraction of α particles has a very interesting behavior: It has a minimum at intermediate densities ($\rho_B \sim 10^{-3}\rho_0$), but then it increases with decreasing density, and completely dominates at low densities. For this fixed entropy a large binding energy of α particles is very important for the thermodynamical balance in the system. Therefore, α particles can be preferable instead of individual nucleons at the low density conditions. The production of α clusters may help to revive the shock wave by maintaining a sufficiently high temperature behind the shock.

The mass distributions of nuclei evolve strongly along the isentropic trajectories. In Fig. 16 we demonstrate this evolution in stellar matter with a large electron fraction $Y_e = 0.4$ for two cases corresponding to a low entropy $S/B=1$, and to a higher entropy $S/B=4$, where the contribution of heavy fragments is still essential. It is important that in the first case ($S/B=1$) at high baryon density ($\rho_B = 0.1\rho_0$) and temperature ($T = 3.39$ MeV), the distribution of heavy nuclei is centred around $A \sim 130$ and has a large width $\sigma_A \sim 50$. Therefore, heavy nuclei with mass number higher than 200, as well as very small clusters, coexist in the system. With decreasing density the distribution of nuclei shifts to smaller masses and becomes more narrow. Finally, the distribution moves into the iron region, where the binding energy is maximal. At higher entropy ($S/B=4$) we have an opposite situation. The masses of produced nuclei become larger with decreasing density. And at very low densities the nuclei reach finally the iron region. The reason for this interesting behavior is that the temperature drops essentially (from 10 to 1 MeV, as seen from Fig. 14) along the adiabatic trajectory.

All above discussed trends take also place in the case of isospin asymmetric matter with a small electron fraction, $Y_e = 0.2$, see Fig. 17. Besides of the expected effect of increasing number of free neutrons, we obtain here that more heavy nuclei are produced at the same densities. In the same time these nuclei are very neutron-rich. For example, at $S/B=1$ and $\rho = 0.1\rho_0$, for $Y_e = 0.2$ we have an average charge of big nuclei $\langle Z \rangle/A \approx 0.28$, in comparison with $\langle Z \rangle/A \approx 0.41$ for $Y_e = 0.4$. Because of formation of the unusual heavy nuclei, the temperature is lower for small electron fractions. One can conclude from analysis of Figs. 15, 16, and 17 that clusterization of nuclear matter at low densities should have important consequences for the explosion, at least via the energy balance. However, this effect will be even stronger if we include into consideration the modifications of the weak reaction rates caused by the clustering (see below).

In Fig. 18 we demonstrate the total adiabatic pressure as function of baryon density. As expected, it increases with density, and with entropy. One can see a nearly linear relation between $\ln(P)$ and $\ln(\rho)$. For a fixed entropy this relation is usually expressed as the polytropic equation

$$P \sim \rho^{\Gamma_{ad}}, \quad (19)$$

where Γ_{ad} is an effective adiabatic index. In Fig. 19 we show the behavior of Γ_{ad} as a function of density for two values of entropy per baryon. At $S/B=1$, when heavy nuclei still exist, the adiabatic index is nearly constant and close to $4/3$, which is expected for relativistic electron gas. At $S/B=8$ the Γ_{ad} coefficient shows more interesting behavior: it changes considerably and goes through the maximum. The maximal value of 1.5 is reached around $10^{-4} - 10^{-2}\rho_0$. This corresponds to a change of the pressure slope seen in Fig. 18. This effect is caused by a nearly complete disintegration of nuclei into nucleons, which takes place in this density region (see Fig. 15). The production of heavy nuclei at higher densities, and production of α particles at lower densities, lead to decreasing Γ_{ad} at the both side of the maximum. Matter with $\Gamma_{ad} < 4/3$ can not resist the gravity and, therefore, unstable with respect to gravitational collapse. On the other hand, matter with $\Gamma_{ad} > 4/3$ can provide conditions for outward propagation of the shock wave during the supernova explosion.

Finally, let us consider now the adiabatic sound velocity, $c_s^2 = \partial P / \partial \rho|_s$, which plays an important role in hydrodynamical simulations. For example, when the collective velocity of matter exceeds c_s a shock wave is generated. In Fig. 20 we present the sound velocity along different adiabates. In this case it can be obtained as $c_s^2 = \Gamma_{ad} \cdot P / \rho$. As expected, c_s increases with density. However, in the case of $S/A=8$, there is a peak around $10^{-2}\rho_0$, which is caused by the same physical reasons as the maximum of Γ_{ad} , shown in Fig. 19. We note that a small sound velocity in comparison with the light velocity give a justification for using nonrelativistic formulas for baryonic and nuclear degree of freedom.

6. Possible in-medium modification of nuclear properties.

6.1 Reduction of symmetry energy.

As we have mentioned in section 3 multifragmentation reactions open a unique possibility to investigate clusterization of nuclear matter at subnuclear densities. Recently, the symmetry energy of hot nuclei was extracted from experimental data [23, 37, 38, 39], and it was demonstrated that the γ coefficient, see Eq. (12), is considerably reduced as compared with the values expected for cold isolated nuclei. This effect becomes stronger with increasing excitation energy. For example, in Fig. 21 we show the extracted values of the γ coefficient, which go significantly down with decreasing impact parameter b , i.e., for more and more central collisions. The empirical value of the γ coefficient, approximately 25 MeV, was obtained for isolated nuclei from the liquid-drop description of their binding energies. As one can see, at high excitation energies it drops down to ≈ 15 MeV, and may even lower, as follows from the analysis of ref. [37]. As discussed in refs. [46, 37, 38, 39, 40, 41] this change can be explained by the reduction of the fragment density, modification of the nuclear surface energy, and the influence of nuclear environment.

Now we come back to the comparison of conditions which can be reached in multifragmentation reactions and in supernova explosions. Specifically, in Fig. 22 we demonstrate the similarity of fragment mass distributions for these two physical systems, calculated within the SMM and SMSM using the same description of hot fragments in dense environment. The density and temperature of stellar matter are chosen close to the ones typical for multifragmentation reactions. The electron fraction ($Y_e = 0.2$) corresponds approximately to the deleptonization values obtained at this density. One can see that the evolution of mass distributions with excitation energy and temperature is qualitatively similar for both cases (see also section 4.3 and refs. [2, 56]). The transition from the 'U-shaped' mass distribution to the exponential one, a characteristic feature of the liquid-gas phase transition, is well pronounced in both cases too. However, in the supernova environments much heavier and neutron-rich nuclei can be produced because of screening effect of surrounding electrons. In this figure we also demonstrate how important is to extract reliable information about the symmetry energy of hot nuclei. As one can see from mass yields at 3 MeV per nucleon in top panel, changing γ coefficient from 25 to 15 MeV has practically no effect on the mass distributions of fragments produced in nuclear reactions. As was shown in refs. [40, 57], in nuclear multifragmentation reactions the most noticeable effect is that the isotope distributions become broader at smaller γ . However, the symmetry coefficient γ has a dramatic influence on masses of nuclei produced in supernova environments. One can see from Fig. 22 that much more heavy (and more neutron-rich) nuclei can be formed in this case. This effect makes very likely production of heavy and superheavy nuclei in supernova environments. In the following these hot nuclei should undergo de-excitation, and their decay products may either survive on the surface of a neutron star or be ejected into inter-stellar space. Also they can serve as seeds for subsequent r -process, as discussed in section 4.4. Therefore, studying the multifragmentation reactions in the laboratory is important for understanding how heavy elements were synthesized in the Universe.

6.2 Electron capture rate.

Reduction of the symmetry energy of hot nuclei can be very important for weak processes. Here we consider a typical example related to deleptonization of matter, e.g., the electron capture by nuclei. One should bear in mind that the electron fraction is crucial for dynamics of stellar matter, since the electron pressure dominates at subnuclear densities. The calculation of the electron capture rate, R_e , was carried out with the method suggested in ref. [58]. It is based on an independent particle model and assumes dominance of Gamow-Teller transitions. The electron chemical potential μ_e and the reaction Q -value are the most important energy scales of the capture process. It is clear that the Q -value is directly related to the symmetry energy coefficient γ . A good approximation for the capture rate (per second) on an isolated nucleus is the expression [58]:

$$R_e = \frac{0.693B_g}{t_g} \left(\frac{T}{m_e c^2} \right)^5 \left[F_4(\eta) - 2\xi F_3(\eta) + \xi^2 F_2(\eta) \right], \quad (20)$$

where $t_g = 6146s$, $B_g = 4.6$ represents a typical (Gamow-Teller plus forbidden) matrix element, $\xi = (Q - \delta E)/T$, $\eta = (\mu_e + Q - \delta E)/T$, $\delta E = 2.5$ MeV, and F_k are the relativistic Fermi integrals of order k . It is instructive to normalize per nucleon this rate by taking into account the whole ensemble of heavy nuclei produced in stellar matter: $\langle R_e \rangle = \sum \rho_{AZ} R_e / \rho_B$. Figure 23 demonstrates that the electron capture rate in stellar matter depends very essentially on the symmetry energy of nuclei. One can see that at relatively high densities $\rho_B \sim 0.1\rho_0$ the electron capture rate changes only by 20-50%, if we adopt the reduced symmetry energy coefficient $\gamma \approx 15$ MeV. This is because a high electron chemical potential drives the reaction. However, at small densities (below $10^{-3}\rho_0$), when heavy nuclei with large charge still exist (at least at low temperatures), the effect of reduced γ is dramatic, of two-three orders of magnitude. We note, that at these relatively low densities and temperatures the nuclear chemical equilibrium may already be problematic [59], although some authors keep using it in network calculations [60]. We believe that hot nuclei can interact with each other by neutron exchange in this case. This situation is similar to what we have at higher densities of nuclear matter in multifragmentation reactions. Therefore, the effect of reduction of the symmetry energy observed in multifragmentation may also take place in the supernova environments and be responsible for significant enhancement of weak reaction rates.

Conclusions

We have formulated a statistical approach (SMSM) designed to describe supernova matter at subnuclear densities. It may be applied for a broad variety of stellar processes, including the collapse of massive stars and supernova explosions, clusterization of nuclear matter in the crust of neutron stars, nuclear composition in merging binary stars, etc. The model includes the whole ensemble of nuclear species, as well as photons and leptons (e^- , e^+ , ν , $\bar{\nu}$). The model fully accounts for the nuclear liquid-gas phase transition, which was previously under active investigation in nuclear reactions. In general, we emphasize

a close connection of the processes in stellar matter with multifragmentation reactions studied in laboratories.

We have calculated main thermodynamical characteristics of the stellar matter under different assumption on the lepton fractions. Nuclear degrees of freedom contribute essentially to the energy and the entropy at high densities. Whereas, at low densities and high temperatures the photons and leptons contributions dominate. The nuclear contribution to pressure becomes essential only when nuclei completely dissociate into nucleons. Accordingly, the adiabatic index increases considerably in this region. On the other hand, we have found that the α particle production at low densities and moderate entropies can be an important process, which should be correctly taken into account in the dynamical simulations of the explosion.

The comparison with the Lattimer-Swesty model shows that thermodynamical quantities of the matter, e.g., pressure, are not very different in two models. The reason is that both models treat the leptons and photons in a similar way. Considerable differences appear in the yields of α particles and heavy nuclei. We believe that the SMSM provides more realistic mass and charge distributions of hot nuclei, without any additional constraint on their sizes.

As a result of our calculations, we especially emphasize the evolutionary nature of the mass and charge distributions of produced heavy fragments. These distributions carry important information regarding the nuclear liquid-gas phase transition in the stellar matter. Also these nuclei participate in many processes which determine the energy deposition and dynamics of the collapse and explosion. Motivated by recent findings in nuclear multifragmentation reactions we have analyzed how possible in-medium modifications of nuclear properties, in particular, a reduction of the symmetry energy, can influence the fragment yields and weak processes. We have found that these effects can be very important, e.g., for the electron capture by nuclei, which is responsible for deleptonization of matter. At the same time, they can increase the yield of big neutron-rich nuclei. We have discussed new mechanisms of nucleosynthesis leading to the production of heavy and superheavy nuclei in supernova environments. In particular, the shell effects existing at relatively low temperatures may provide an additional enhancement factor for their formation.

The authors thank W. Trautmann, J. Schaffner-Bielich, M. Hempel, K. Langanke, Th. Janka, J. Lattimer, M. Liebendoerfer, Th. Buervenich, H. Stöcker, and W. Greiner for many fruitful discussions. One of us (A.S.B.) acknowledges financial support from the Helmholtz International Center for FAIR. This work was partly supported by DFG grant 436RUS 113/711/02 (Germany) and by grant NS-3004.2008.2 (Russia).

References

- [1] N. Bohr, Nature, 137 (1936) 344.
- [2] J.P. Bondorf, A.S. Botvina, A.S. Iljinov, I.N. Mishustin, K. Sneppen, Phys. Rep. 257 (1995) 133.

- [3] G.E. Brown, H.A. Bethe and G. Baym, Nucl. Phys. A 375 (1982) 481.
- [4] H.A. Bethe, Rev. Mod. Phys. 62 (1990) 801.
- [5] H.-T. Janka, R. Buras, K. Kifonidis, M. Rampp, T. Plewa, Review in "Core Collapse of Massive Stars", Fryer, C.L. (ed.), astro-ph/0212314 (2001); H.-T. Janka and E. Mueller, Astron. Astrophys. 306 (1996) 167.
- [6] M. Liebendörfer et al., Nucl. Phys. A 719 (2003) 144c; Astrophys. J. 620 (2005) 840.
- [7] K. Sumiyoshi et al., Astrophys. J. 629 (2005) 922.
- [8] A. Burrows et al., Astrophys. J. 640 (2006) 878.
- [9] H.-Th. Janka, A. Marek, B. Mueller, L. Schec, arXiv:0712.3070 [astro-ph] (2007); AIP Conf. Proc. 983 (2008) 369.
- [10] F.K. Sutaria, A. Ray, J.A. Sheikh, P. Ring, Astron. Astrophys. 349 (1999) 135.
- [11] W.R. Hix et al., Phys. Rev. Lett. 91 (2003) 201102.
- [12] K. Langanke, G. Martinez-Pinedo, Nucl. Phys. A 673 (2000) 481.
- [13] C.J. Horowitz, Phys. Rev. D 55 (1997) 4577.
- [14] J.J. Cowan, F.-K. Thieleman, J.W. Truran, Phys. Rep. 208 (1991) 267.
- [15] Yong-Zhong Qian, Prog. Part. Nucl. Phys. 50 (2003) 153.
- [16] D.Q. Lamb, J.M. Lattimer, C.J. Pethick, D.G. Ravenhall, Nucl. Phys. A 360 (1981) 459; J.M. Lattimer, C.J. Pethick, D.G. Ravenhall, D.Q. Lamb, Nucl. Phys. A 432 (1985) 646.
- [17] J.M. Lattimer, F.D. Swesty, Nucl. Phys. A 535 (1991) 331.
- [18] H. Shen, H. Toki, K. Oyamatsu, K. Sumiyoshi, Nucl. Phys. A 637 (1998) 435.
- [19] C. Ishizuka, A. Ohnishi, K. Sumiyoshi, Nucl.Phys. A 723 (2003) 517.
- [20] A.S. Botvina, I.N. Mishustin, Phys. Lett. B 584 (2004) 233.
- [21] A. Aprahamian, K. Langanke, M. Wiescher, Prog. Part. Nucl. Phys. 54 (2005) 535.
- [22] R.Buras et al., astro-ph/0507135 (2005).
- [23] A.S. Botvina, I.N. Mishustin, Phys. Rev. C 72 (2005) 048801.
- [24] G. Sauer, H. Chandra, U. Mosel, Nucl.Phys. A 264 (1976) 221.
- [25] D.Q. Lamb, J.M. Lattimer, C.J. Pethick, D.G. Ravenhall, Phys. Rev. Lett. 41 (1978) 1623.

- [26] D.G. Ravenhall, C.J. Pethick, J.R. Wilson, Phys. Rev. Lett. 50 (1983) 2066.
- [27] C.J. Pethick, D.G. Ravenhall, Annu. Rev. Nucl. Part. Sci. 45 (1995) 429.
- [28] C.J. Horowitz, M.A. Perez-Garcia, J. Piekarewicz, Phys. Rev. C 69 (2004) 045804.
- [29] G. Watanabe, K. Sato, K. Yasuoka, T. Ebisuzaki, Phys. Rev. C 69 (2004) 055805.
- [30] A.S. Botvina, A.S. Iljinov, I.N. Mishustin, Nucl. Phys. A 507 (1990) 649.
- [31] A.S. Botvina et al., Nucl. Phys. A 584 (1995) 737.
- [32] R.P. Scharenberg et al., Phys. Rev. C 64 (2001) 054602.
- [33] M. D'Agostino et al., Phys. Lett. B 371 (1996) 175.
- [34] N. Bellaize et al., Nucl. Phys. A 709 (2002) 367.
- [35] S.P. Avdeyev et al., Nucl. Phys. A 709 (2002) 392.
- [36] M. D'Agostino et al., Nucl. Phys. A 650 (1999) 329.
- [37] A. Le Fevre et al., Phys. Rev. Lett. 94 (2005) 162701.
- [38] J. Iglio et al., Phys. Rev. C 74 (2006) 024605.
- [39] G. Souliotis et al., Phys. Rev. C 75 (2007) 011601(R).
- [40] A.S. Botvina et al., Phys. Rev. C 74 (2006) 044609.
- [41] N. Buyukcizmeci, A.S. Botvina I.N. Mishustin, R. Ogul, Phys. Rev. C 77 (2008) 034608.
- [42] A.S. Botvina et al., Nucl. Phys. A 475 (1987) 663.
- [43] A.V. Ignatiuk et al., Phys. Lett. B 76 (1978) 543.
- [44] M. Prakash et al., Phys. Rep. 280 (1997) 1.
- [45] A.S. Botvina, A.S. Iljinov, I.N. Mishustin, Sov. J. Nucl. Phys. 42 (1985) 712.
- [46] A.S. Botvina, O.V. Lozhkin, W. Trautmann, Phys. Rev. C 65 (2002) 044610.
- [47] K.A. Bugaev, M.I. Gorenstein, I.N. Mishustin, Phys. Lett. B 498 (2001) 144.
- [48] A.S. Botvina, I.N. Mishustin, Phys. Rev. C 63 (2001) 061601(R).
- [49] M. Bender, K. Rutz, P.-G. Reinhardt, J.A. Maruhn, W. Greiner, Phys. Rev. C 60 (1999) 034304.
- [50] J.R. Nix, Ann. Rev. Nucl. Sci. 22 (1972) 65.

- [51] T.J. Buervenich, I.N. Mishustin, W. Greiner, Phys. Rev. C 76 (2007) 034310.
- [52] A.S. Botvina, I.N. Mishustin, W. Greiner, work in progress.
- [53] G.J. Mathews, P. Marronetti, J.R. Wilson, Phys. Rev. D 58 (1998) 043003.
- [54] T.A. Thompson, A. Burrows, B.S. Meyer, Astrophys. J. 562 (2001) 887.
- [55] T. Ohnishi, Astroph. & Space Sci. 69 (1980) 155.
- [56] A.S. Botvina, I.N. Mishustin, Phys. At. Nucl. 71 (2008) 1088.
- [57] N. Buyukcizmeci, R. Ogul, A.S. Botvina, Eur. Phys. J. A 25 (2005) 57.
- [58] K. Langanke et al., Phys. Rev. Lett. 90 (2003) 241102.
- [59] A.S. Botvina, I.N. Mishustin, work in progress.
- [60] C. Travaglio et al., Astron. Astrophys. 425 (2004) 1029.

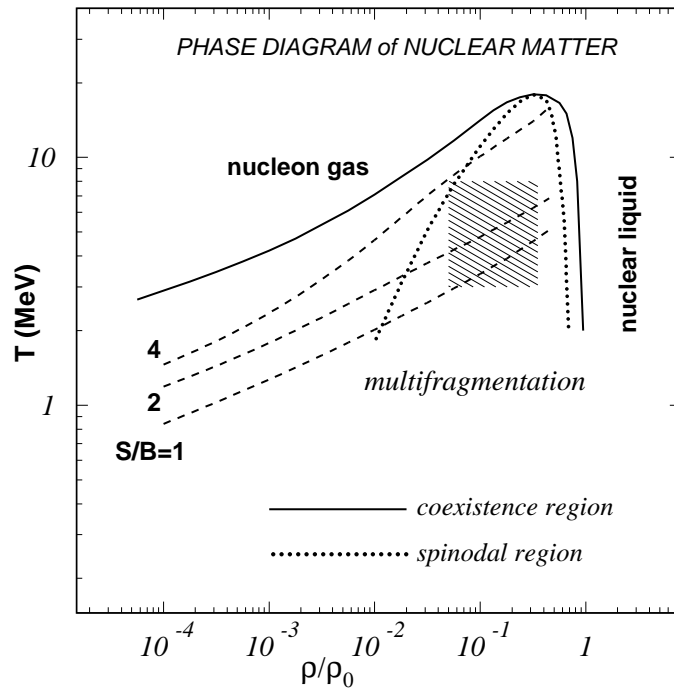


Figure 1: Nuclear phase diagram on the 'temperature – baryon density' plane. Solid and dotted lines indicate boundaries of the liquid-gas coexistence region and the spinodal instability region. The shaded area corresponds to typical conditions for nuclear multifragmentation reactions. The dashed lines are isentropic trajectories characterized by constant entropy per baryon, $S/B = 1, 2$, and 4.

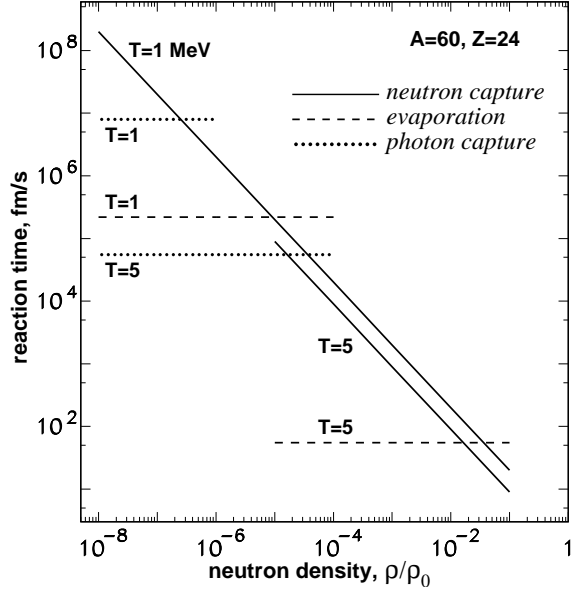


Figure 2: Estimated reaction rates for a typical nucleus, with mass number $A=60$ and charge $Z=24$, in stellar environment versus the density of free neutrons. Different lines correspond to different reaction types as indicated in the figure. Temperatures T (in MeV) are given at the lines.

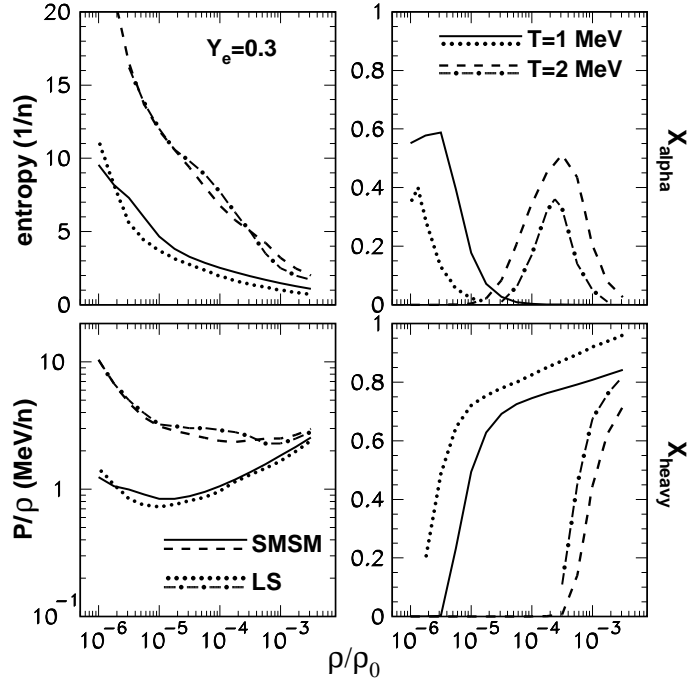


Figure 3: Comparison of SMSM and the Lattimer-Swesty (LS) model [17] for stellar matter with electron fraction $Y_e=0.3$ and temperatures $T = 1$ and 2 MeV, as functions of the baryon density in units of the normal nuclear density $\rho_0 \approx 0.15 \text{ fm}^{-3}$. The panels present the total entropy per nucleon, the pressure divided by density, the fractions of α -particles and heavy nuclei ($A > 4$).

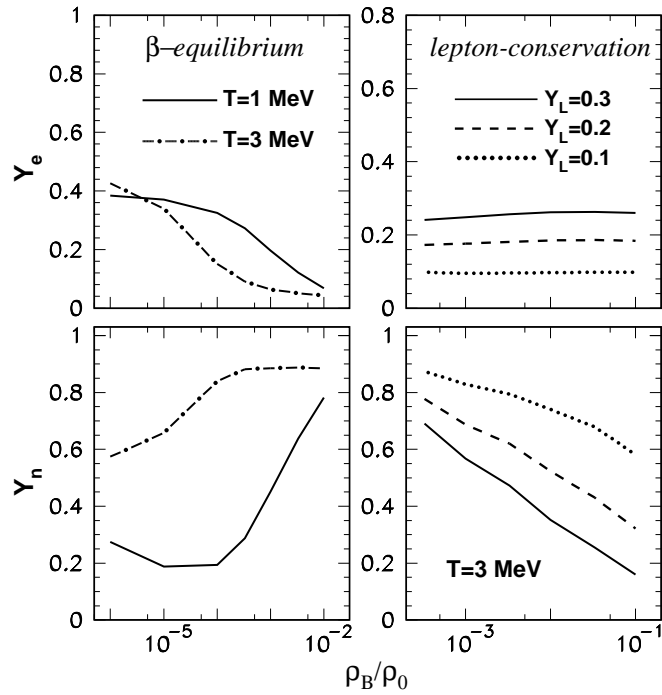


Figure 4: Average fractions of electrons Y_e (top panels) and free neutrons Y_n (bottom panels) versus baryon density in units of ρ_0 . Left panels present results for the β -equilibrated matter with $T = 1$ and 3 MeV. Right panels correspond to the conserved lepton fractions $Y_L=0.1$, 0.2 and 0.3, and $T = 3$ MeV.

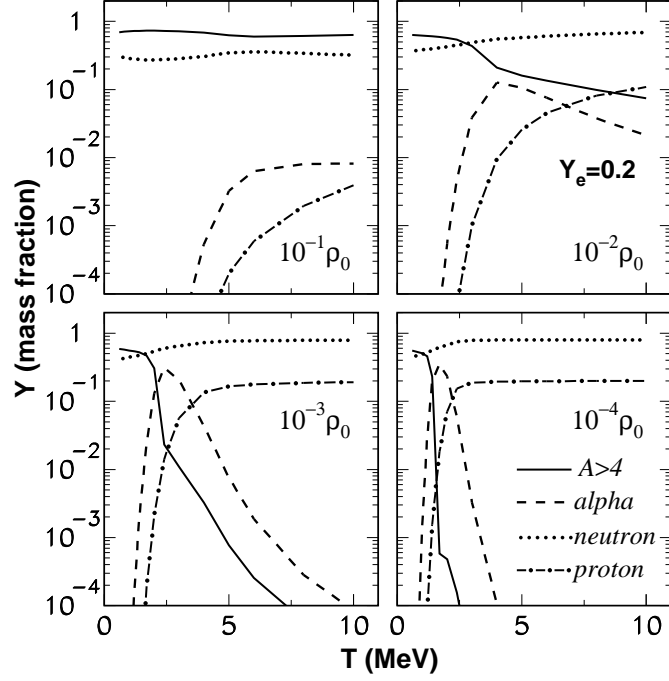


Figure 5: Mass fractions of nuclear species for stellar matter at $Y_e=0.2$ as functions of temperature. Solid lines are for heavy nuclei ($A > 4$), dashed lines – α -particles, dotted lines – neutrons, dot-dashed lines – protons. The results for baryon densities of 10^{-1} , 10^{-2} , 10^{-3} , $10^{-4}\rho_0$ are presented in the corresponding panels.

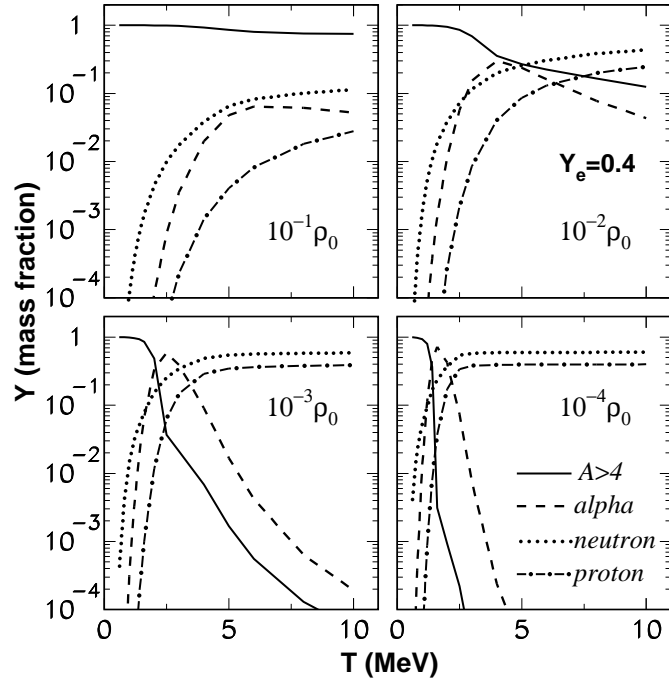


Figure 6: The same as Fig. 5 but at $Y_e=0.4$.

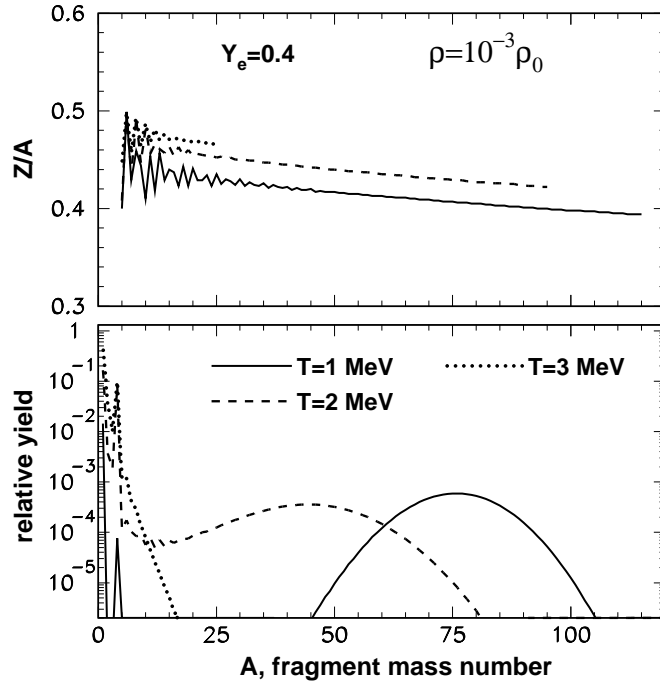


Figure 7: Mass distributions, i.e., yields per nucleon, (bottom panel) and average charge to mass-number ratios (top panel) for nuclei produced at density $10^{-3}\rho_0$ and $Y_e=0.4$, for temperatures $T=1, 2$ and 3 MeV.

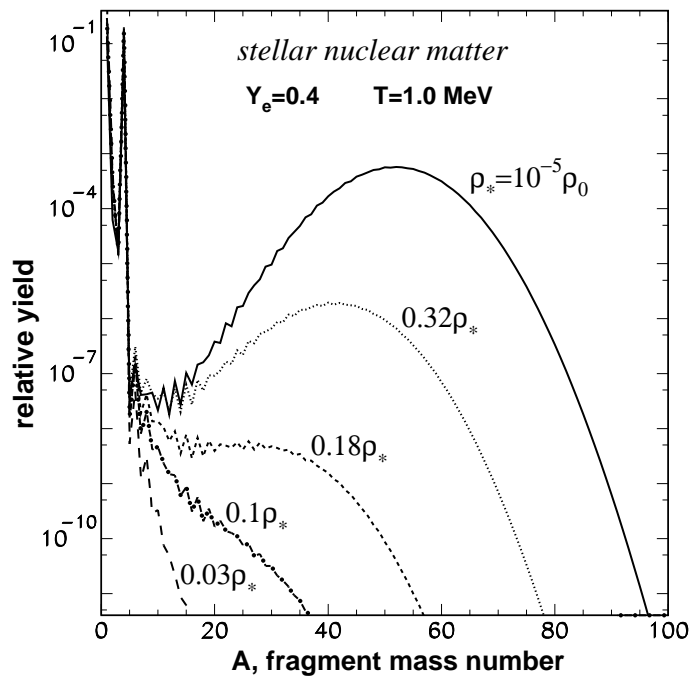


Figure 8: Fragment mass distributions (yields per nucleon) at $T=1$ MeV and several densities in units of $\rho_* = 10^{-5}\rho_0$ (see notations at the lines). Electron fraction is $Y_e=0.4$.

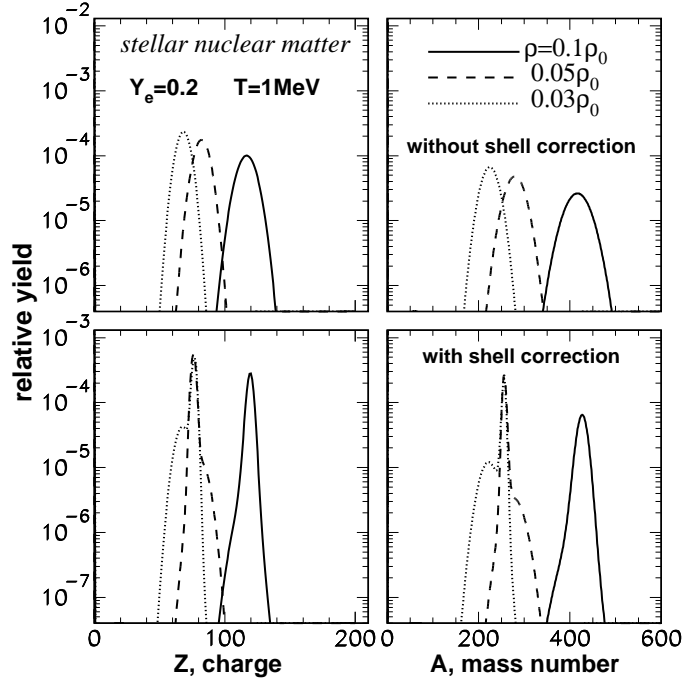


Figure 9: Mass (right panels) and charge (left panels) distributions of superheavy nuclei at subnuclear densities without (top panels) and with (bottom panels) shell corrections. The stellar matter has electron fraction $Y_e=0.2$ and temperature $T=1$ MeV. Different lines correspond to different densities as indicated in the figure.

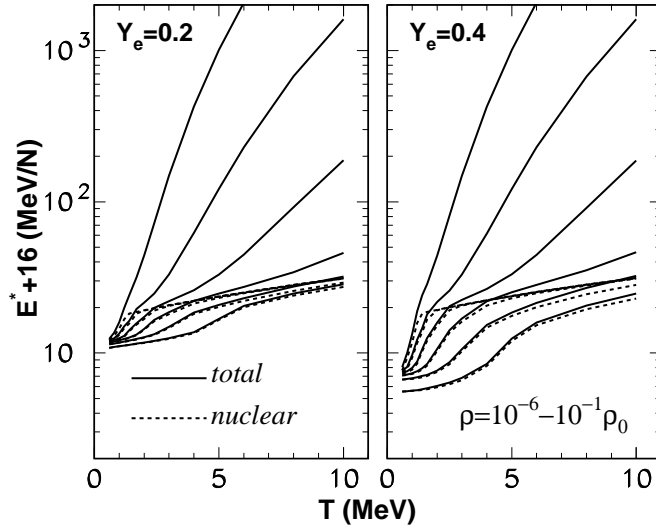


Figure 10: Energy per nucleon as function of temperature in stellar environment with electron fractions $Y_e=0.2$ (left) and $Y_e=0.4$ (right), measured from the binding energy of normal nuclear matter (16 MeV per nucleon). Dashed lines show only contributions of nuclei. Solid lines give total energies including nuclear, electron and photon contributions. Baryon densities of 10^{-6} , 10^{-5} , 10^{-4} , 10^{-3} , 10^{-2} , and $10^{-1}\rho_0$, correspond to the 6 lines from the top to the bottom in the both panels.

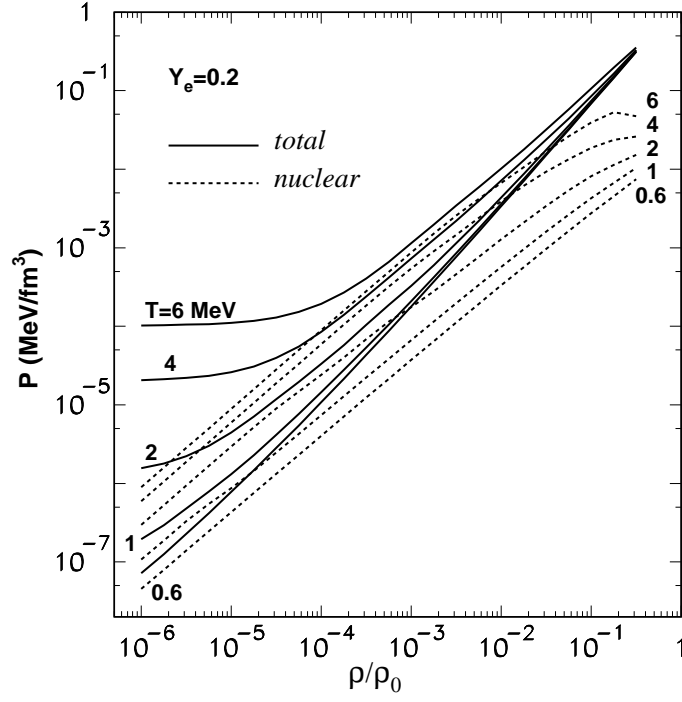


Figure 11: Pressure as function of baryon density in units ρ_0 (the phase diagram in the $P - \rho$ plane) for $Y_e=0.2$. Dashed lines are only nuclear contributions, solid lines are total pressures including also electron and photon contributions. The temperatures of 6, 4, 2, 1, and 0.6 MeV, are presented by different lines from the top to the bottom.

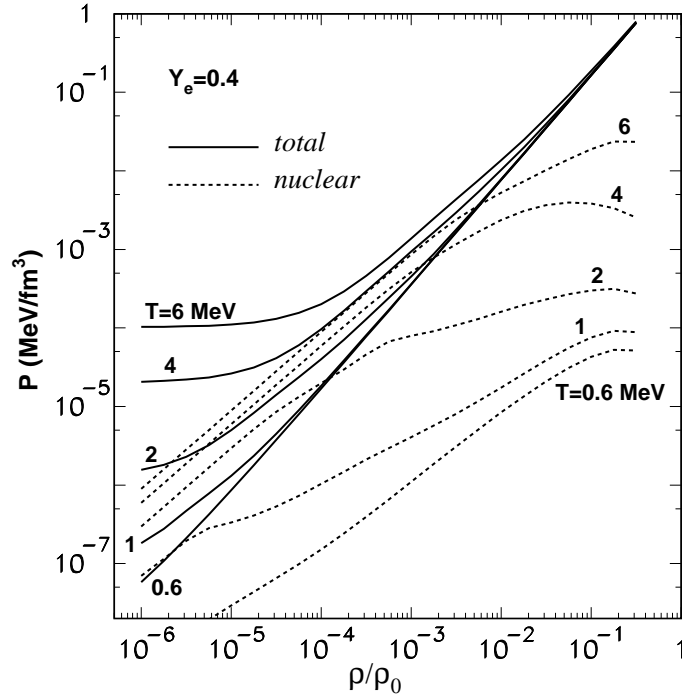


Figure 12: The same as Fig. 11 but for $Y_e=0.4$.

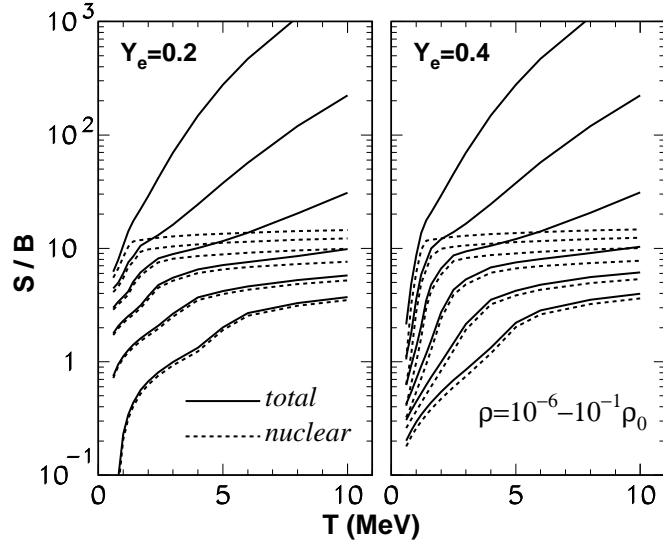


Figure 13: Entropy (per baryon) of stellar matter as function of temperature, for electron fractions $Y_e=0.2$ (left) and $Y_e=0.4$ (right). Dashed lines show only nuclear contributions, solid lines give total entropy including also electron and photon contributions. The densities of 10^{-6} , 10^{-5} , 10^{-4} , 10^{-3} , 10^{-2} , and $10^{-1}\rho_0$, correspond to the 6 lines from the top to the bottom in the both panels.

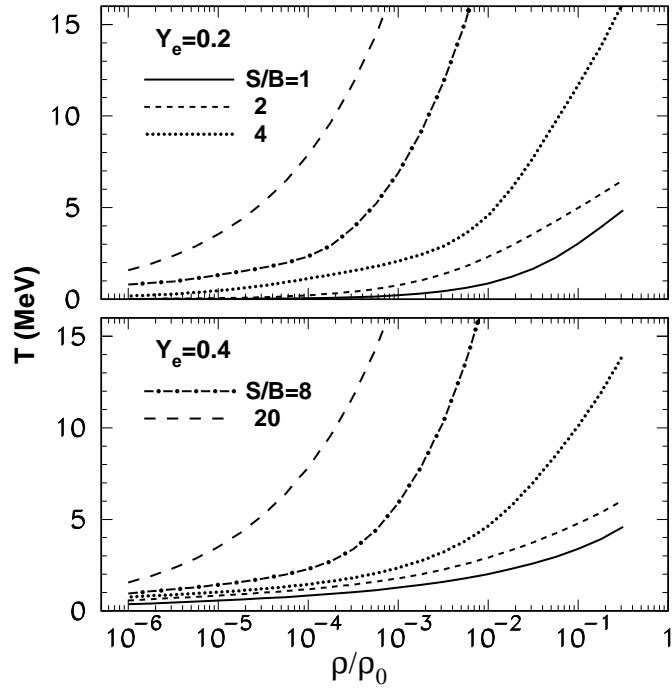


Figure 14: Isentropic trajectories on the 'temperature - baryon density' plane for different entropy per baryon values ($S/B=1, 2, 4, 8, 20$) indicated in the figure. Electron fractions are $Y_e=0.2$ (top) and $Y_e=0.4$ (bottom).

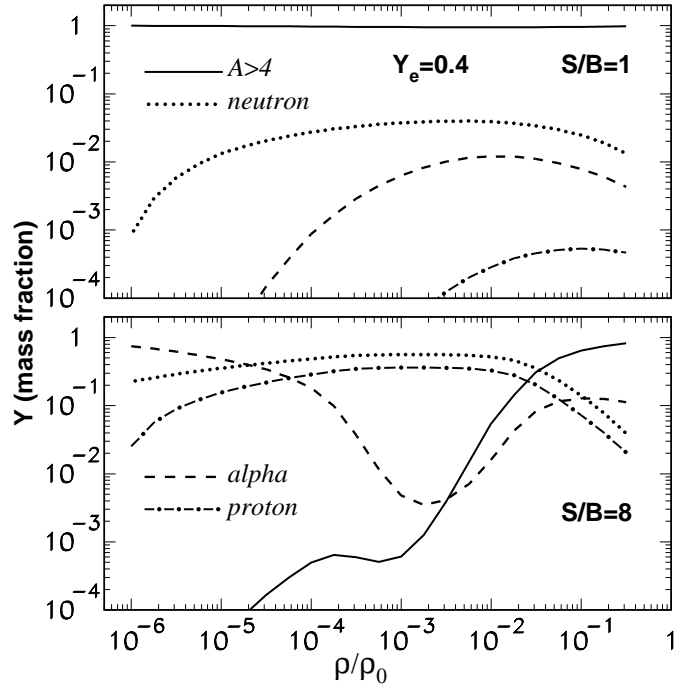


Figure 15: Mass fractions of nuclear species along isentropes with $S/B=1$ (top) and 8 (bottom), for $Y_e=0.4$. Solid, dotted, dashed, and dot-dashed lines correspond to heavy nuclei ($A > 4$), neutrons, α -particles, and protons, respectively.

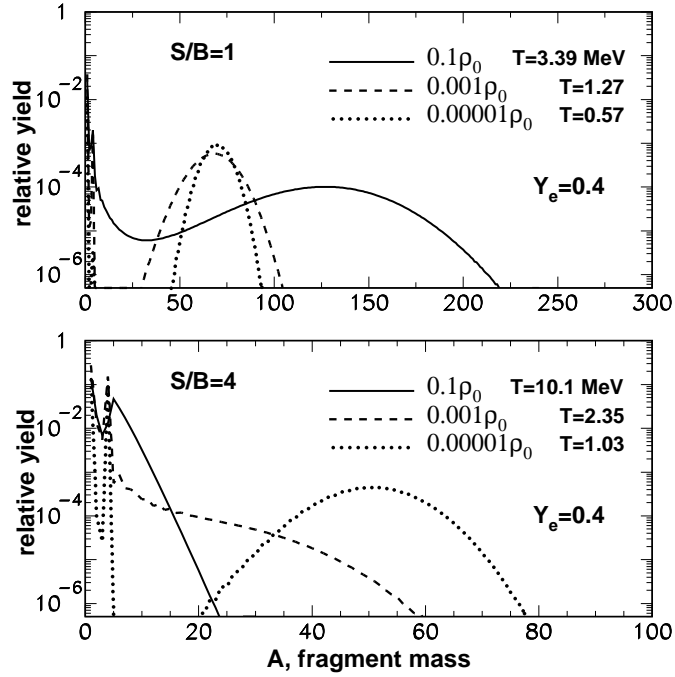


Figure 16: Mass distributions of nuclei along isentropic trajectories with $S/B=1$ (top) and 4 (bottom), for $Y_e=0.4$. Different lines correspond to specific baryon densities and temperatures (in MeV), as indicated in the figure.

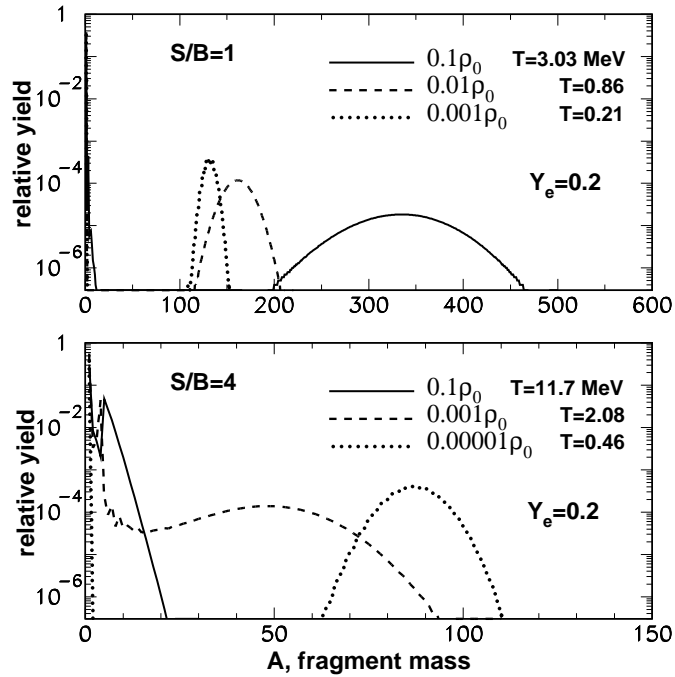


Figure 17: The same as Fig. 16 but for $Y_e=0.2$.

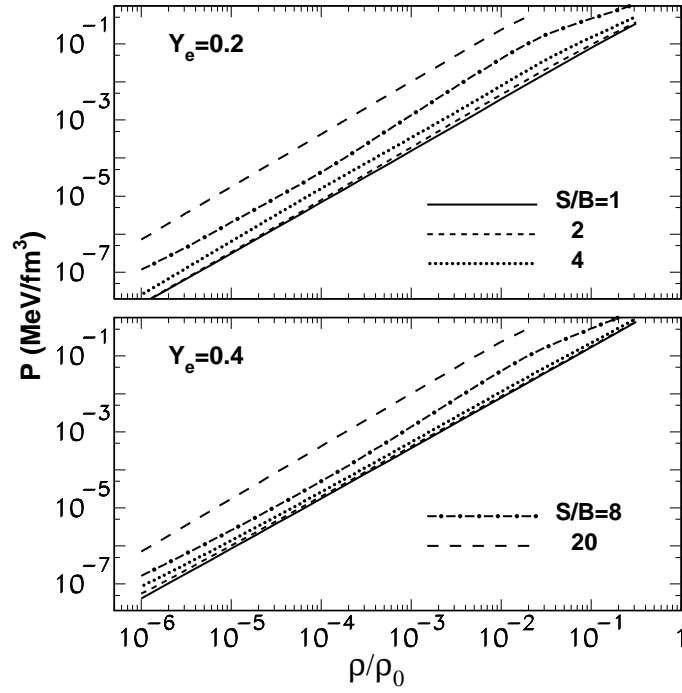


Figure 18: Adiabatic pressure as function of baryon density (in units of ρ_0), for $Y_e=0.2$ (top) and $Y_e=0.4$ (bottom). Different lines correspond to entropies per baryon $S/B=1, 2, 4, 8,$ and 20 units, as indicated in the figure.

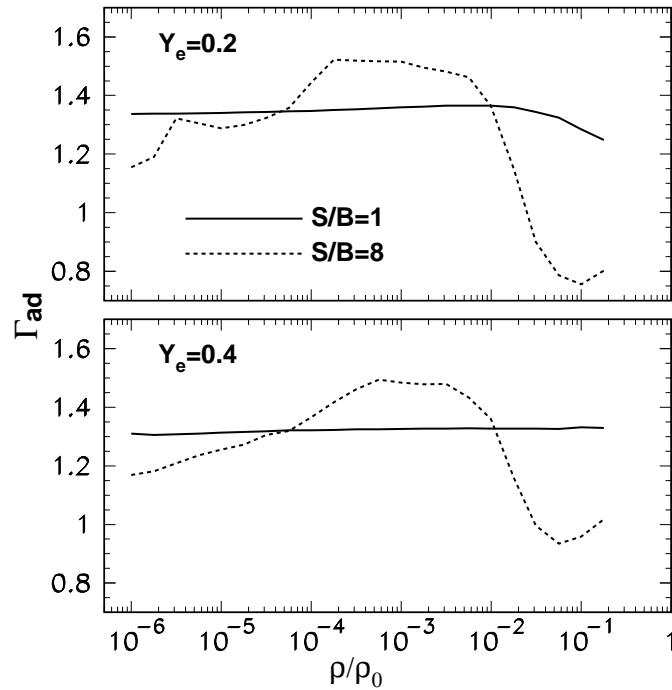


Figure 19: Adiabatic index as function of baryon density at $S/B=1$ (solid lines) and $S/B=8$ (dashed lines), for $Y_e=0.2$ (top) and $Y_e=0.4$ (bottom).

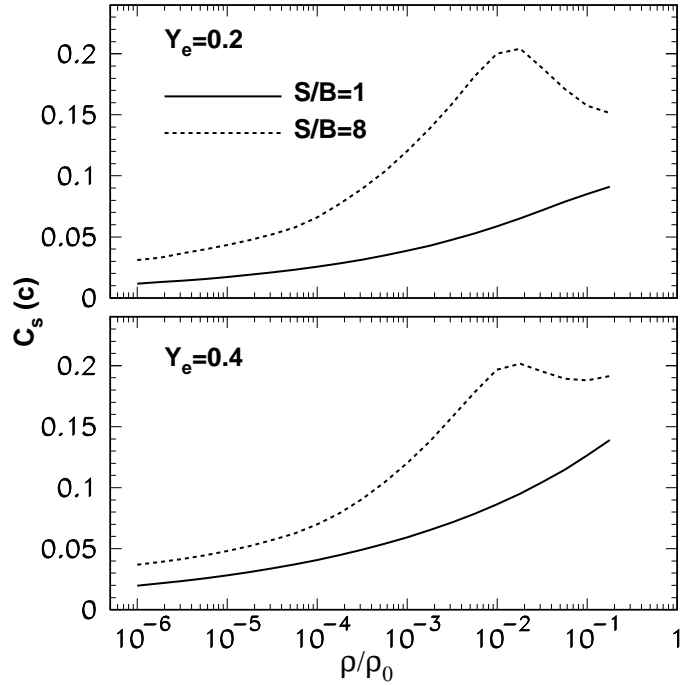


Figure 20: Adiabatic sound velocity c_s (in units of light velocity) at $S/B=1$ (solid lines) and $S/B=8$ (dashed lines), for $Y_e=0.2$ (top) and $Y_e=0.4$ (bottom).

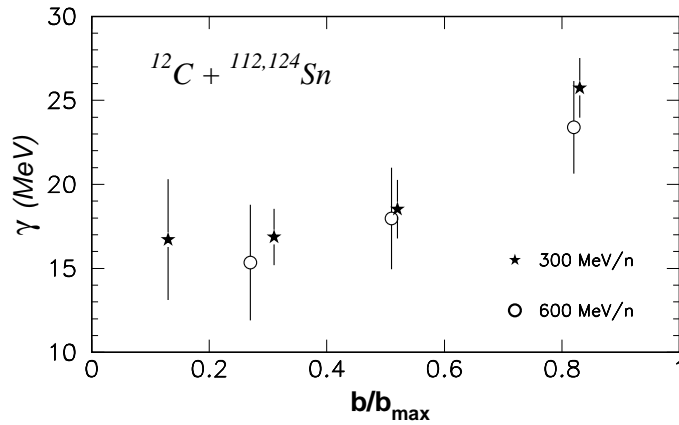


Figure 21: The apparent symmetry energy coefficient γ of hot nuclei, as extracted from multifragmentation of tin isotopes induced by ^{12}C beams with energy 300 and 600 MeV per nucleon, versus relative impact parameter b/b_{max} [37].

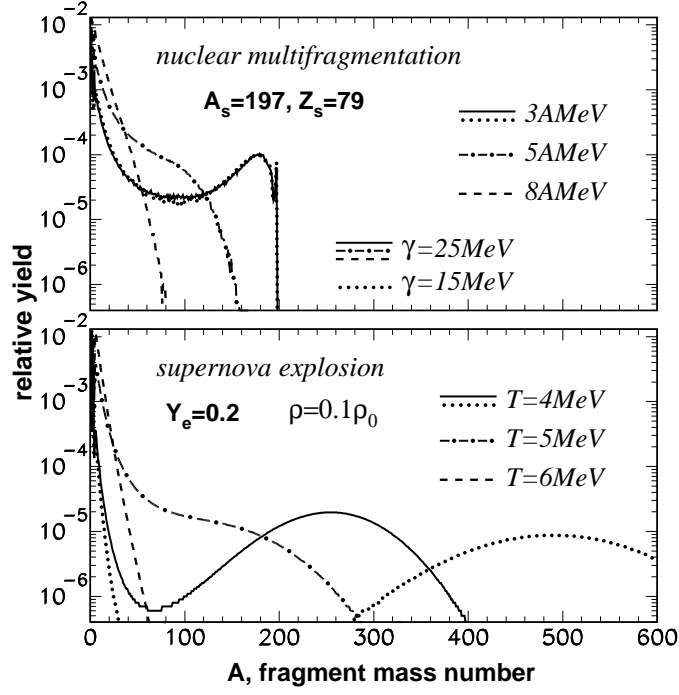


Figure 22: Fragment mass distributions (yields per nucleon) in multifragmentation of Au sources (top panel) and in supernova environment at the electron fraction $Y_e = 0.2$ and baryon density $0.1\rho_0$ (bottom panel). The calculations at excitation energies of 3, 5, and 8 MeV per nucleon (top), and different temperatures T (bottom), are shown by different curves. Effects of the reduced symmetry energy coefficient γ are also demonstrated in both panels.

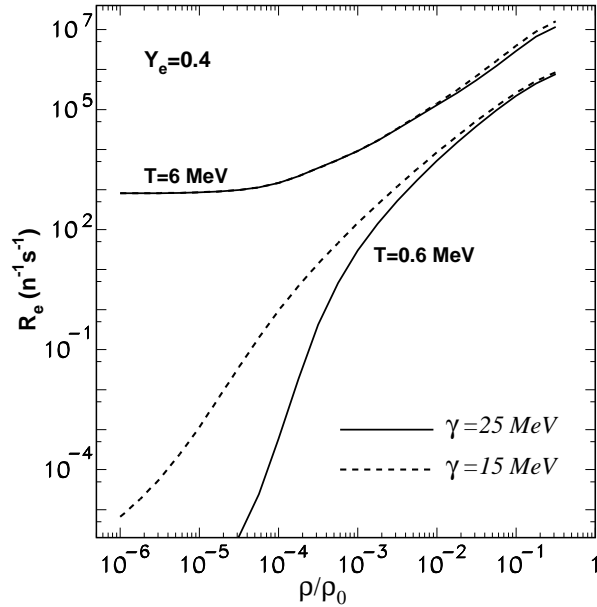


Figure 23: Density dependence of electron-capture rates R_e on hot nuclei in supernova environment at different temperatures T and the electron fraction $Y_e = 0.4$. Solid and dashed lines show results for standard (25 MeV) and reduced (15 MeV) values of symmetry energy coefficients γ .